

# Organic Thin Film Transistors Based on Cyclohexyl-Substituted Organic Semiconductors

Jason Locklin,<sup>†,‡,§</sup> Dawen Li,<sup>§</sup> Stefan C. B. Mannsfeld,<sup>‡</sup> Evert-Jan Borkent,<sup>§</sup> Hong Meng,<sup>§</sup> Rigoberto Advincula,<sup>\*,†</sup> and Zhenan Bao<sup>\*,‡</sup>

*Department of Chemistry, University of Houston, 136 Fleming Building, Houston, Texas 77204,*

*Department of Chemical Engineering, Stanford University, 381 North South Mall,*

*Stanford, California 94305, and Bell Labs, Lucent Technologies, Murray Hill, New Jersey 07974*

Received December 9, 2004. Revised Manuscript Received April 19, 2005

Various cyclohexyl end-capped oligomeric semiconductors based on oligothiophene, oligothiophene-fluorene, and perylene diimide have been synthesized using Stille and Suzuki coupling. These materials exhibit increased solubility over their unsubstituted and hexyl-substituted counterparts and have been successfully employed as the active component in organic field-effect transistors. The morphology of vacuum-deposited films made with these oligomers has been investigated using atomic force microscopy (AFM), transmission electron microscopy (TEM), and X-ray diffraction (XRD). Field effect mobility as high as 0.17 cm<sup>2</sup>/V·s was observed in fluorene-thiophene oligomers deposited at elevated substrate temperatures. With the series of materials, a correlation between the size of the endgroup with respect to the size of the inner semiconducting core of the molecule is found to be an important factor in orienting the molecules with their long axis perpendicular to the substrate surface in the thin film phase, and directly related to charge transport in these materials.

## Introduction

Conjugated oligomers and polymers represent one of the most important classes of advanced materials in recent years. The extensive amounts of research in the field are driven by the promise of low-cost processing applications that are typical of organic materials over their inorganic counterparts. The greatest advantage of organic materials is the diversity of structures and tunability of properties offered through molecular design. Recently, great strides have been made in areas such as thin-film transistors,<sup>1,2</sup> light-emitting diodes,<sup>3</sup> photovoltaic cells,<sup>4,5</sup> and nonlinear optical devices.<sup>6</sup>

Typically, organic semiconductors are divided into two major classes: conjugated polymers and their corresponding oligomers. In both classes of materials, it has been demonstrated that efficiency of charge transport is directly related to long-range packing of molecules in semiconductor films. The classic example of electrical properties being dominated by molecular order is that of FETs based on an oligomeric sexithiophene as demonstrated by Servet and Garnier.<sup>7</sup> The

authors demonstrated that molecular design could be used to control the packing arrangement of molecules in the thin film phase and the field-effect mobility in the device was improved by a factor of 50 by controlling the molecular order in the evaporated film. This important characteristic of oligomeric materials has since been demonstrated in other conjugated systems.<sup>8,9</sup>

Another important aspect of conjugated oligomers is that they are monodisperse with respect to molecular weight and can be considered as models for conducting polymers in which structure–property relationships can be obtained with respect to electronic, photonic, thermal, and morphological properties of their corresponding polydisperse high-molecular-weight analogues. In fact, monodispersed oligomers have also been used to elucidate the folding properties of polymers.<sup>10</sup>

To date, the best FET mobilities reported for oligomeric semiconductors are higher than those obtained with conjugated polymers. Almost all of the high-performance oligomers in the literature involve straight alkyl chain functionalization at the  $\alpha$ - and  $\omega$ -ends of the conjugated ring system that allows for a perpendicular arrangement of the oligomers with respect to the substrate surface. In this work, we intend to explore the effect of different endgroups on the morphology and FET performance. We demonstrate a general trend

\* Authors to whom correspondence should be addressed. E-mail: radvincula@uh.edu, zbao@stanford.edu.

<sup>†</sup> University of Houston.

<sup>‡</sup> Stanford University.

<sup>§</sup> Lucent Technologies.

- (1) Horowitz, G. *Adv. Mater.* **1998**, *10*, 365.
- (2) Katz, H. E.; Lovinger, A. J.; Johnson, J.; Kloc, C.; Siegrist, T.; Li, W.; Lin, Y. Y.; Dodabalapur, A. *Nature* **2000**, *404*, 478.
- (3) Burroughes, J. H.; Bradley, D. D. C.; Brown, A. R.; Marks, R. N.; Mackay, K.; Friend, R. H.; Burn, P. L.; Holmes, A. B. *Nature* **1990**, *347*, 539.
- (4) Sariciftci, N. S.; Smilowitz, L.; Heeger, A. J.; Wudl, F. *Science* **1992**, *258*, 1474.
- (5) Yu, G.; Gao, J.; Hummelen, J. C.; Wudl, F.; Heeger, A. J. *Science* **1995**, *270*, 1789.
- (6) Bredas, J. L.; Adant, C.; Tackx, P.; Persoons, A. *Chem. Rev.* **1994**, *94*, 243.

- (7) Servet, B.; Horowitz, G.; Ries, S.; Lagorse, O.; Alnot, P.; Yassar, A.; Deloffre, F.; Srivastava, P.; Hajlaoui, P.; Lang, P.; Garnier, F. *Chem. Mater.* **1994**, *6*, 1809.
- (8) Grundlach, J. B.; Lin, Y. Y.; Jackson, T. N.; Nelson, S. F.; Schlom, D. G. *IEEE Electron Device Lett.* **1997**, *18*, 87.
- (9) Katz, H. E.; Lovinger, A. J.; Dodabalapur, A. *Chem. Mater.* **1996**, *8*, 2542.
- (10) Nelson, J. C.; Saven, J. G.; Moore, J. S.; Wolynes, P. G. *Science* **1997**, *277*, 1793.

in the use of cyclohexyl end-capping groups with several different conjugated oligomeric systems that yield good performance in thin film devices. The cyclohexyl group adds steric bulkiness at the periphery of the molecule that provides for improved solubility without having a detrimental effect on the molecular packing in the thin film phase. Also, with the series of materials, we observe a correlation between the size of the endgroups with respect to the semiconducting core of the molecule and how it relates to the thin film phase crystal structure of vacuum-deposited ultrathin films at different substrate temperatures.

## Experimental Section

**Chemicals and Methods.** All chemical reagents were purchased from Aldrich Chemical Co. unless otherwise stated. Solvents were purchased from Fisher. Tetrahydrofuran (THF) was distilled over sodium/benzophenone ketyl, and *N,N*-dimethylformamide (DMF) was purchased anhydrous or otherwise dried over Linde type 4-Å molecular sieves.

**Instrumentation.** Nuclear magnetic resonance (NMR) spectra were recorded on a General Electric QE-300 spectrometer at 300 MHz for  $^1\text{H}$  NMR and 75 MHz for  $^{13}\text{C}$  NMR. Chemical shifts ( $\delta$ ) are reported in parts per million and the residual solvent peak was used as an internal standard.

**X-ray Diffraction Measurements.** For morphological characterizations, the materials were deposited onto Si/SiO<sub>2</sub> wafers simultaneously with the FET devices. The X-ray diffraction studies were collected in reflection mode on a Scintag XDS2000 diffractometer at room temperature equipped with Peltier germanium solid-state detector in the  $2\theta$  range 3–110° with a step size of 0.02°, and a step time of 10 s.

**Microscopy Techniques.** The same samples used for X-ray diffraction were examined in ambient conditions by AFM with a PicoSPM II (PicoPlus, Molecular Imaging) in the magnetic AC mode (MAC mode). MAC mode uses a magnetic field to drive a magnetically coated cantilever in the top-down configuration. Type II MAC-levers with a spring constant of 2.8 nN/M with about 10-nm tip radius were used for all scans. In situ annealing was performed inside an environmental chamber (N<sub>2</sub> atmosphere) with a PicoSPM II in contact mode using a Lakeshore temperature controller (donated by Molecular Imaging) from 25 to 250 °C. A temperature ramp of 5 °C/min was used that provided excellent imaging conditions at temperatures above 100 °C. Additionally, the film morphology and in-plane crystal structure were determined using a JEOL transmission electron microscope. Films 400 Å thick were deposited on carbon-coated TEM grids and diffraction images of these films were recorded at a primary electron beam energy of 100 kV.

**Oligomer Synthesis.** The synthetic protocol for the oligomers used in this work is outlined in Scheme 1.

**Synthesis of 2-Cyclohexyl-9H-fluorene.** A Grignard reagent of cyclohexylmagnesium bromide, prepared by the reaction of cyclohexyl bromide (9.45 g, 58 mmol) with Mg (1.53 g, 63 mmol) in ether (100 mL), was added dropwise into a solution of 2-bromo-9H-fluorene (13.83 g, 56.5 mmol) in ether (100 mL) containing 1,3-bis(diphenylphosphino)propane]dichloronickel (II) (Ni(dppp)<sub>2</sub>Cl<sub>2</sub>) (0.16 g, 0.3 mmol) as catalyst over a period of 30 min. After stirring for 20 h, the reaction mixture was quenched with 0.1 M HCl and extracted with ether. The combined ether solution was washed with H<sub>2</sub>O three times and dried over anhydrous MgSO<sub>4</sub>. After removal of the solvent, the resulting white powder was subjected to purification by flash chromatography using silica gel with hexane as the eluent (8.7 g, yield, 62%).  $^1\text{H}$  NMR (300 MHz, CDCl<sub>3</sub>),  $\delta_{\text{H}}$

7.78 (d,  $J = 7.0$  Hz, 1 H), 7.72 (d,  $J = 7.5$  Hz, 1 H), 7.54 (d,  $J = 7.5$  Hz, 1 H), 7.43 (s, 1 H), 7.40–7.24 (m, 3 H), 3.88 (s, 2 H), 2.61 (m, 1 H), 1.98–1.79 (m, 4 H), 1.54–1.31 (m, 6 H).  $^{13}\text{C}$  NMR (75 MHz, CDCl<sub>3</sub>),  $\delta_{\text{C}}$  143.16, 139.52, 126.58, 126.15, 125.52, 124.90, 123.41, 122.65, 119.62, 119.54, 44.81, 36.87, 34.72, 26.98, 26.21 ppm.

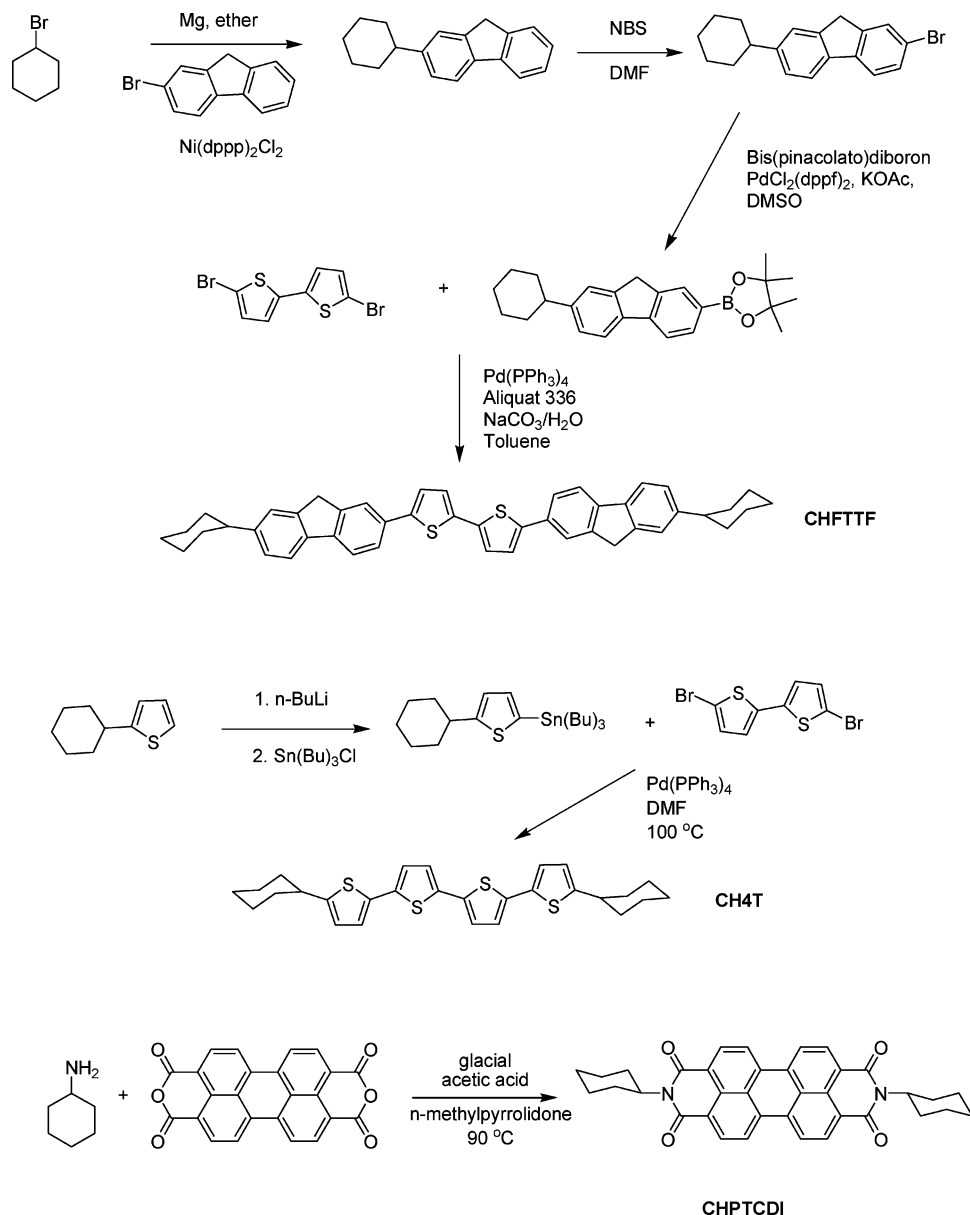
**Synthesis of 2-Bromo-7-cyclohexyl-9H-fluorene.** *N*-Bromosuccinimide (NBS) (1.02 g, 5.7 mmol) in DMF was added by addition funnel to 2-cyclohexyl-9H-fluorene (1.3 g, 5.2 mmol) in DMF (total volume ~50 mL) at room temperature in the dark and stirred overnight. The mixture was then poured into ice water (250 mL). The precipitate was filtered, washed with methanol, and dried in air. The crude product was subjected to flash chromatography using silica gel with hexanes as the eluent. Evaporation of the solvent resulted in 1.62 g of white powder (yield, 98%).  $^1\text{H}$  NMR (300 MHz, CDCl<sub>3</sub>),  $\delta_{\text{H}}$  7.66 (d,  $J = 8.0$  Hz, 2 H), 7.59 (d,  $J = 8.0$  Hz, 1 H), 7.47 (dd,  $J = 7.8, 1.1$  Hz, 1 H), 7.38 (s, 1 H), 7.23 (dd,  $J = 7.8, 1.1$  Hz, 1 H), 3.85 (s, 2 H), 2.57 (m, 1 H), 1.90–1.75 (m, 4 H), 1.52–1.25 (m, 6 H).  $^{13}\text{C}$  NMR (75 MHz, CDCl<sub>3</sub>),  $\delta_{\text{C}}$  145.09, 143.02, 140.73, 138.41, 133.47, 129.63, 128.07, 125.77, 123.42, 120.79, 119.84, 119.71, 44.69, 36.63, 34.65, 26.91, 26.15 ppm.

**Synthesis of 2-(7-Cyclohexyl-9H-fluoren-2-yl)-4,4,5,5-tetramethyl-1,3,2-dioxaborolane.** A nitrogen-flushed three-neck round-bottom flask was charged with 2-bromo-7-hexyl-9H-fluorene (1.1 g, 3.4 mmol), bis(pinacolato)diboron (0.94 g, 3.7 mmol), potassium acetate (0.99 g, 10.2 mmol), and [1,1'-bis(diphenylphosphino)ferrocene]dichloropalladium (8 mg, 0.02 mmol), complex with dichloromethane (1:1). Dimethyl sulfoxide (DMSO, 40 mL) was then added, and the mixture was bubbled with nitrogen for 15 min. After the reaction mixture was heated at 80 °C for 16 h, it was cooled to room temperature and poured into ice-water (200 mL). It was then extracted with CH<sub>2</sub>Cl<sub>2</sub> (20 mL  $\times$  3) and the combined organic layer was dried over anhydrous magnesium sulfate. The solvent was removed by rotary evaporation and the residue was passed through a flash silica gel column with hexane/methylene chloride (v/v, 1:1) as the eluent to give white crystals (0.79 g, yield 63%).  $^1\text{H}$  NMR (300 MHz, CDCl<sub>3</sub>),  $\delta_{\text{H}}$  7.97 (s, 1 H), 7.81 (dd,  $J = 7.6$  Hz, 1H), 7.73 (m, 2H), 7.40 (s, 1H), 7.22 (dd,  $J = 7.8$  Hz, 1H), 3.86 (s, 2H), 2.55 (m, 1H), 1.93–1.74 (m, 4H), 1.50–1.19 (m, 18H).

**Synthesis of 5,5'-Bis-(7-cyclohexyl-9H-fluoren-2-yl)-2,2'-bithiophene (CHFTTF).** To a solution of 2-(7-cyclohexyl-9H-fluoren-2-yl)-4,4,5,5-tetramethyl-1,3,2-dioxaborolane (0.76 g, 2.0 mmol) and 2,2'-dibromobithiophene (0.33 g, 1.0 mmol) dissolved in toluene (5 mL) was added sodium carbonate (1.08 g, 10 mmol) dissolved in water (5 mL) followed by the addition of phase-transfer agent Aliquot 336 (0.4 g, 1 mmol). The mixture was bubbled with nitrogen for 15 min, then tetrakis(triphenylphosphine)palladium(0) (80 mg, 0.069 mmol) was added. The mixture was heated to 85 °C for 48 h under nitrogen. The reaction mixture was cooled to room temperature and poured into methanol (100 mL). The yellow precipitate was filtered off, then washed with water, dilute acid (5% HCl), and water again. The crude product was washed with hot methanol and hot acetone three times (100 mL  $\times$  3) to remove the starting material as well as the possible monosubstituted byproduct. The product was further purified by three vacuum sublimations to give a bright yellow powder (0.55 g, yield 82%).  $^1\text{H}$  NMR (300 MHz, CDCl<sub>3</sub>),  $\delta_{\text{H}}$  7.97 (s, 2H), 7.83 (d, 2H), 7.74 (d, 2H), 7.70 (d, 2H) 7.62 (m, 2H), 7.40 (m, 4H), 7.22 (d, 2H) 3.91 (s, 4H), 2.57 (m, 2H), 1.95–1.75 (m, 8H), 1.50–1.21 (m, 12H). Elemental analysis found: C, 82.44; H, 6.25; S, 9.40. Calcd for C<sub>46</sub>H<sub>42</sub>S<sub>2</sub>: C, 83.84; H, 6.42; S, 9.73.

**Synthesis of 2-Cyclohexylthiophene.** A Grignard reagent of cyclohexylmagnesium chloride, prepared by the reaction of cyclo-

Scheme 1. Synthesis Scheme of Various Cyclohexyl Endcapped Oligomers Used in This Work



hexyl chloride (5.34 g, 45 mmol) with Mg (1.02 g, 42 mmol) in ether (100 mL), was added dropwise into a solution of 2-bromothiophene (6.36 g, 39 mmol) in ether (75 mL) containing 1,3-bis(diphenylphosphino)propane]dichloronickel (II) ( $\text{Ni}(\text{dppp})_2\text{Cl}_2$ ) (0.16 g, 0.3 mmol) as catalyst over a period of 30 min. After stirring for 20 h, the reaction mixture was quenched with 0.1 M HCl and extracted with ether. The combined ether solution was washed with  $\text{H}_2\text{O}$  three times and dried over anhydrous  $\text{MgSO}_4$ . After removal of the solvent, the resulting liquid was subjected to purification by flash chromatography using silica gel with hexane as the eluent (3.4 g, yield 53%).  $^1\text{H}$  NMR (300 MHz,  $\text{CDCl}_3$ ),  $\delta_{\text{H}}$  7.15 (dd,  $J = 5.2, 1.1$  Hz, 1 H), 6.97 (dd,  $J = 5.2, 4.6$  Hz, 1 H), 6.85 (dd,  $J = 4.6, 1.1$  Hz, 1H), 2.88 (m, 1 H), 2.11–1.76 (m, 4 H), 1.48–1.34 (m, 6 H).  $^{13}\text{C}$  (75 MHz,  $\text{CDCl}_3$ ),  $\delta_{\text{C}}$  152.26, 126.33, 122.043, 121.631, 39.30, 35.45, 26.44, 25.90.

**Synthesis of Tributyl-(5-cyclohexyl-thiophen-2-yl)stannate.** BuLi (2.5 M in hexane) (7.6 mL, 19 mmol) was added to a solution of 2-cyclohexylthiophene (3.0 g, 18 mmol) in THF at  $-78$  °C. After lithiation, tributyltin chloride (6.18 g, 19 mmol) was added to the mixture. The reaction was allowed to warm to room temperature for 3 h. After normal workup, the product was used without further

purifications (yield, 90% by NMR).  $^1\text{H}$  NMR (300 MHz,  $\text{CDCl}_3$ ),  $\delta_{\text{H}}$  7.01 (d,  $J = 3.3$  Hz, 1 H), 6.93 (d,  $J = 3.3$  Hz, 1 H), 2.86 (m, 1 H), 2.11–1.81 (m, 4 H), 1.61–1.54 (m, 6 H), 1.48–1.31 (m, 12 H), 1.12–1.06 (m, 6 H), 0.91 (t,  $J = 6.9$  Hz, 9 H).

**Synthesis of 5,5''-Dicyclohexyl-[2,2';5',2'';5'',2''']quaterthiophene (CH4T).** Tributyl-(5-cyclohexyl-thiophen-2-yl)stannate (3.57 g, 7.8 mmol), 5,5'-dibromo-[2,2']bithiophene (1.20 g, 3.7 mmol), and  $\text{Pd}(\text{PPh}_3)_4$  (15 mg, 0.1 mol %) were added to DMF (~25 mL) in a one-neck flask equipped with a condenser. After three freeze–pump–thaw cycles, the solution was heated to 100 °C for 24 h. After the mixture was cooled to room temperature, it was filtered and washed with hexane and THF to remove starting material and any monocoupled product. The product was Soxhlet extracted with  $\text{CHCl}_3$  overnight to remove residual catalyst (1.51 g, yield 84%).  $^1\text{H}$  NMR (300 MHz,  $\text{CDCl}_3$ ),  $\delta_{\text{H}}$  7.06 (d,  $J = 3.9$  Hz, 2H), 7.02 (d,  $J = 3.9$  Hz, 2H), 6.73 (m, 4H), 2.81 (m, 2H), 2.09 (m, 4H), 1.86 (m, 4H), 1.75 (m, 6H), 1.53–1.28 (m, 6H). Elemental analysis found: C, 67.93; H, 6.07; S, 26.01. Calcd for  $\text{C}_{28}\text{H}_{30}\text{S}_4$ : C, 68.07; H, 6.11; S, 25.92

**Synthesis of *N,N'*-Bis(cyclohexyl)perylene-3,4,9,10-tetracarboxyldiimide (CHPTCDI).** A mixture of perylene-3,4,9,10-tetra-

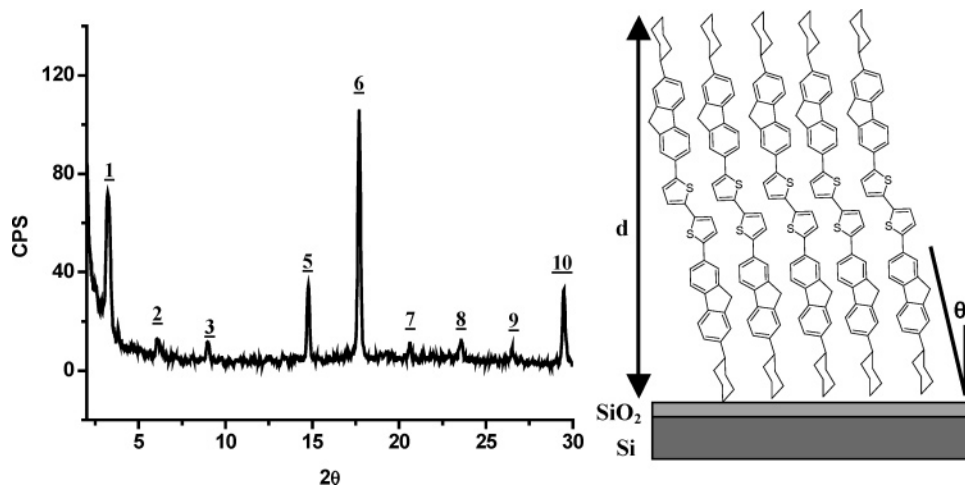


**Figure 1.** X-ray diffraction data acquired for a 400-Å-thick film of **CHFTTF** deposited at a substrate temperature of 130 °C (left). The peak at  $2\theta = 3.1^\circ$  is assigned as the first order and a  $d$ -spacing of 29.9 ( $\pm 0.6$ ) Å is obtained from the average of all the successive reflections assigned above. The tilted orientation of **CHFTTF** is represented schematically on the right for one molecular layer.

carboxylic dianhydride (10 g, 25.5 mmol), cyclohexylamine (7.6 g, 76.5 mmol), and glacial acetic acid (0.2 g) was charged into a one-neck flask with *n*-methylpyrrolidone (100 mL). The solution was heated to 90 °C for 20 h. After cooling to room temperature, the precipitated product was filtered, washed with methanol, acetone, and ethyl acetate, and Soxhlet extracted with  $\text{CHCl}_3$  for 48 h to remove excess starting material.  $^1\text{H}$  NMR (300 MHz,  $\text{CDCl}_3$ )  $\delta_{\text{H}}$  (Ar-H show AB2 splitting pattern) 8.65 (d,  $J = 8.1$ , 4H), 8.59 (d,  $J = 8.1$ , 4H), 5.05 (m, 2H), 2.62–2.50 (m, 4 H), 1.92 (m, 4H), 1.63 (m, 6H), 1.49–1.26(m, 6H). Elemental analysis found: C, 77.96; H, 5.45; N, 5.05; O, 11.54. Calcd for  $\text{C}_{36}\text{H}_{30}\text{N}_2\text{O}_4$ : C, 76.74; H, 5.38; N, 4.91; O, 11.08.

**FET Device Fabrication.** Both the “top” and “bottom” contact configurations were used to make the FET devices similar to those previously reported in the literature.<sup>2,5</sup> The *n*-doped silicon substrate functions as the gate electrode. A 3000-Å silicon dioxide dielectric layer with a capacitance per unit area ( $C_i$ ) of  $1.1 \times 10^{-8}$  F/cm<sup>2</sup> was thermally grown on the gate substrate. For the “top” contact geometry, gold electrodes were deposited after the semiconductor deposition by using shadow masks with a  $W/L$  varying from 6 to 20, where  $L = 40$ – $200$   $\mu\text{m}$ . The semiconductor layer was then deposited over the entire electrode/dielectric surface. The organic semiconductors were deposited at a rate of 0.5–1 Å/s under a pressure of  $\sim 5.0 \times 10^{-7}$  Torr to a final thickness of 400 Å determined by a quartz crystal monitor in the evaporation chamber. The substrate temperature during deposition was controlled by heating a copper block where the substrate was mounted. The electrical characteristics were obtained at room temperature in air using a 4145B Hewlett-Packard (HP) semiconductor parameter analyzer. For the “bottom” contact geometry, gold electrodes forming channels of 250- $\mu\text{m}$  width ( $W$ ) and 1.5–25- $\mu\text{m}$  length ( $L$ ) were photolithographically defined. A solution of the semiconductor in the appropriate solvent was then drop-cast or spin-coated over the entire substrate surface.

## Results and Discussion

**Synthesis.** The synthesis of the cyclohexyl-encapped oligomers was carried out through a series of cross-coupling reactions that involved Suzuki or Stille coupling. The synthetic routes and corresponding structures are shown in Scheme 1. It is worth noting that the yield from Grignard/Kumada coupling of 2-bromofluorene or 2-bromothiophene with bromocyclohexane was lower than expected due to the

difficulty in forming the cyclohexylmagnesium bromide species. Also, in the synthesis of **CH4T**, coupling of lithiated thiophene with bromocyclohexane was attempted but unsuccessful due to the inaccessibility of backside attack possibly because of the bromine group being in an equatorial position, effectively locking the ring in a chair configuration.

All of the oligomers were characterized by  $^1\text{H}$  NMR and elemental analysis and the results were consistent with the predicted chemical structures. All the oligomers are moderately soluble in chloroform and other halogenated solvents at room temperature. **CHFTTF** has the lowest solubility ( $\sim 1$  mg/mL in  $\text{CHCl}_3$  at room temperature) of the three oligomers, but its solubility is greater than that of the unsubstituted and hexyl-substituted version of the same molecule.<sup>5</sup> **CHPTC-DI** has a solubility of  $\sim 1.5$  mg/mL in  $\text{CHCl}_3$  at room temperature. **CH4T** is the most soluble in chloroform ( $\sim 2$  mg/mL at room temperature) and is also soluble in other nonpolar solvents such as toluene, cyclohexane, dioxane, and benzene. This is twice as soluble as that reported for a dihexyl-version of 4T. Before device fabrication, the materials were purified by sublimation under vacuum ( $10^{-4}$  Torr) at least twice to reduce impurities that might cause charge traps or unwanted dopants in the oligomeric semiconductor layer.

**Morphology.** Figure 1 shows the X-ray diffractogram of **CHFTTF** films grown on top of 3000-Å-thick  $\text{SiO}_2$  films thermally grown on highly doped Si  $\langle 100 \rangle$  substrates at a substrate temperature of 130 °C. The diffractograms were taken in the reflection geometry using Ni-filtered Cu  $K\alpha$  radiation at a scanning rate of 0.5°  $2\theta/\text{min}$ . The films revealed narrow, intense peaks with multiple orders of reflection consistent with a single preferred orientation. The peak at  $2\theta = 3.1^\circ$  is assigned as the first-order reflection and the remaining peaks are successive orders of reflections. The average  $d$ -spacing from the 10 diffractions is 29.9 Å with a standard deviation of 0.6 Å. This is consistent with layers that are a single molecule thick. A tilt angle of 21° can be calculated from the idealized length of 32.1 Å (based on energy minimization with MM2) which does not account for the interdigitation of endgroups between layers. The

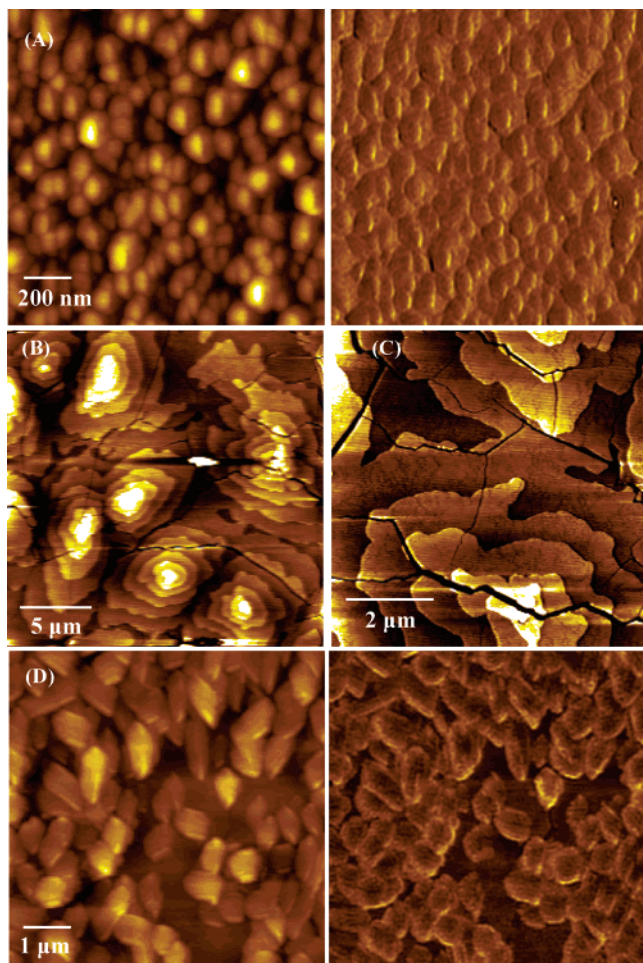


**Figure 2.** MAC mode AFM images of 40-nm CHFTTF films deposited onto Si/SiO<sub>2</sub> at (a) 25 °C (topography and phase), (b) 130 °C (topography, 20 × 20 μm), (c) 130 °C (topography, 7 × 7 μm), and (d) 150 °C (topography and phase).

amount of crystallinity in the films depends strongly on the substrate temperature ( $T_{\text{sub}}$ ) during deposition. At substrate temperatures below 75 °C, there was very little crystallinity observed in the films (no orders of diffraction at  $T_{\text{sub}} = 25$  °C and  $2\theta = 3.07$ ,  $d = 28.7$  Å at  $T_{\text{sub}} = 75$  °C). Multiple orders of diffracted beams were seen at  $T_{\text{sub}} = 115$ , 130, and 140 °C with a  $d$  spacing consistent with that shown in Figure 1. The film deposited at  $T_{\text{sub}} = 150$  °C showed two peaks ( $2\theta = 3.22$ ,  $d = 27.4$  Å, and  $2\theta = 17.6$ ,  $d = 5.0$  Å).

Figure 2 shows the magnetic-AC (MAC-mode) AFM of 400-Å-thick films of CHFTTF deposited at (a) 25 °C (topography and phase), (b) 130 °C (topography, 20 × 20 μm), (c) 130 °C (topography, 7 × 7 μm), and (d) 150 °C (topography and phase). The morphology of the film deposited at 25 °C consists of very small and homogeneous grains with an average diameter of about 70 nm. Increasing the substrate temperature during deposition results in a substantial increase in size of the grains in which molecules are closely packed parallel to each other in a vertical arrangement (with their long axes nearly perpendicular) with respect to the substrate. This packing arrangement allows faster growth in directions parallel to the layers than perpendicular to them, so that the crystals form thin plates with a terraced structure as the molecules form multiple layers. The step height between layers for Figure 2c is 29 Å

as determined by AFM and is in good agreement with the interlayer spacing deduced from X-ray analysis, confirming the existence of single-molecule-thick layers in an end-on orientation. At 130 °C, some of the grains are larger than 10 μm which is exceptionally large in an organic semiconductor thin film. Cracks in terraced grains (as shown in Figure 2c) were observed, possibly due to the mismatch in thermal expansion coefficient between the SiO<sub>2</sub> substrate and the organic semiconductor (see Figure 4). Postannealing of the film from 25 to 250 °C was attempted with in-situ AFM in contact mode to “heal” the cracks but there was no observable change in morphology.

If the substrate temperature during deposition is increased to 150 °C, the underlying molecules grow parallel to the substrate in a vertical arrangement (not shown in the image) but a significant amount grow perpendicular, and their presence probably induces a lowering of charge transport, as seen below by the decrease in mobility. It is unclear from the image the exact orientation of the outermost layers or if nucleation of these defects arises from crystallization between grain boundaries of underlying layers. At such a high  $T_{\text{sub}}$ , other factors such as temperature-activated competing processes that result in nucleation of the bulk phase or surface diffusion limits may play a role.<sup>11</sup> A similar behavior has been observed with a hexyl-substituted F3TF and with unsubstituted oligothiophenes.<sup>5,12</sup> This may account for the overall decrease in crystallinity observed in the X-ray measurements at this temperature.

We have also probed the film morphology and in-plane structure of CHFTTF at  $T_{\text{sub}} = 120$  °C using TEM (Figure 3). It can be seen that the film is formed by extended, single crystalline grains with typical diameters of 3–5 μm. Figure 3b shows a TEM diffraction image recorded from the large grain in the center of Figure 3a (illuminated circular area) at a primary beam energy  $V_0 = 100$  kV. The diffraction pattern corresponds to a rectangular in-plane (parallel to the substrate surface) unit cell with dimensions of  $a = 9.6$  Å,  $b = 5.6$  Å. The large number of visible higher diffraction order spots corroborates the high crystal perfection of the probed grain. Considering the area of the rectangular unit cell, it is highly likely that it actually contains *two* CHFTTF molecules. Furthermore, there are systematic absences of the (h0) and (0k) odd order diffraction spots in the diffraction image (see white circles) which can be explained by a “herringbone” alignment of these two molecules in the rectangular unit cell with a (nearly) p2gg plane symmetry group.<sup>13,14</sup> Such an arrangement is depicted in the lower-right inset which represents a top-view scheme of the in-plane unit cell. For the plane symmetry group to be p2gg, the second molecule is required to be located in the center of the unit cell while the azimuthal angles of the two molecules need to have equal absolute values with opposing signs ( $-\Phi$  and  $\Phi$ ). However,

- (11) Ruiz, R.; Choudhary, D.; Nickel, B.; Toccoli, T.; Chang, K.-C.; Mayer, A.; Clancy, P.; Blakey, J. M.; Headrick, R. L.; Iannotta, S.; Malliaras, G. *Chem. Mater.* **2004**, *16*, 4497.
- (12) Horowitz, G.; Hajlaoui, M. E. *Adv. Mater.* **2000**, *12*, 1046.
- (13) Ertl, G.; Küppers, J. *Low Energy Electrons and Surface Chemistry*; VCH Verlagsgesellschaft: Weinheim, 1985.
- (14) Clarke, L. J. *Surface Crystallography*; John Wiley & Sons Ltd: New York, 1985.

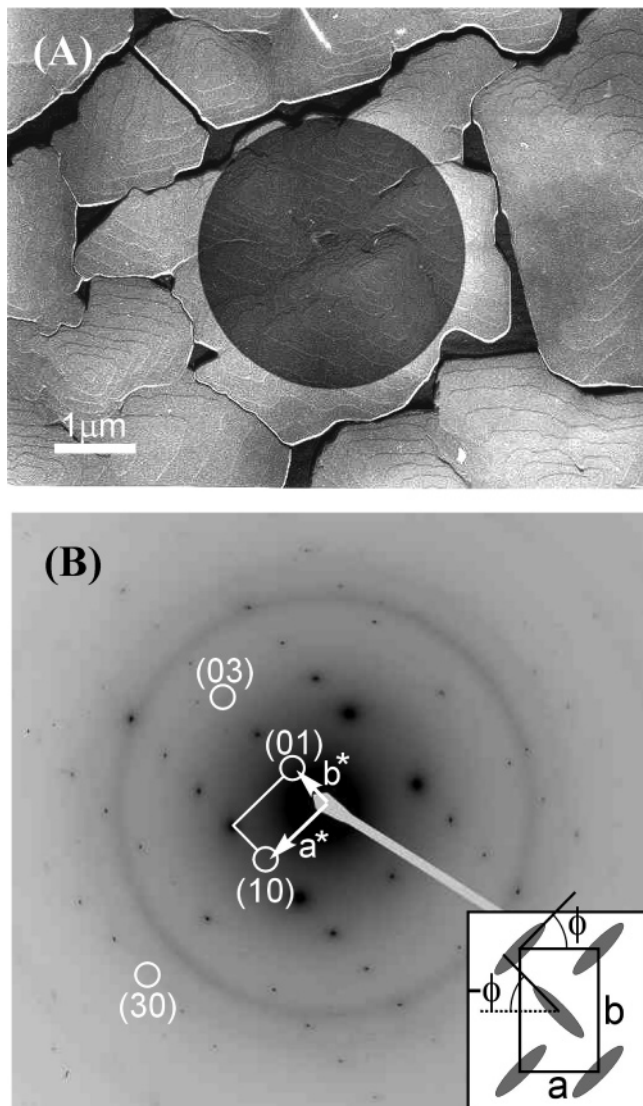


**Figure 3.** (A) TEM image of a 400-Å-thick **CHFTTF** film showing large, single crystalline grains. The gray circle in the center corresponds to the area illuminated by the electron beam while the diffraction image shown in (B) was obtained. (B) TEM diffraction image ( $V_0 = 100$  kV). The diffraction pattern corresponds to a rectangular in-plane unit cell (lower-right inset) with two molecules per unit cell. From the apparent weak intensity of odd order the  $(h0)$  and  $(0k)$  diffraction spots a herringbone-like arrangement of the two molecules in the unit cell can be concluded.

the symmetry of the actual in-plane unit cell cannot be *exactly* as sketched in the inset of Figure 3b ( $p2gg$ ) because the long molecule axis exhibits a tilt with respect to the substrate surface plane (as discussed above). Furthermore, the **CHFTTF** molecule itself lacks the required “internal” mirror symmetry (i.e., the electron density is slightly anisotropic in both sides of the molecule defined by the long molecule axis).<sup>13</sup> Still, the observed very weak intensity of odd order diffraction spots is a clear indication for a herringbone type in-plane arrangement close to that sketched in Figure 3b.

Increasing  $T_{\text{sub}} = 140$  °C during deposition of **CHFTTF** does not alter the crystal structure of the film, but yields an interconnected film morphology with very large crystalline grains. Figure 4 also shows several fractures observed within the large crystalline grains (small dark gaps). Unlike the dark grain boundaries visible in Figure 3a, the gaps in Figure 4

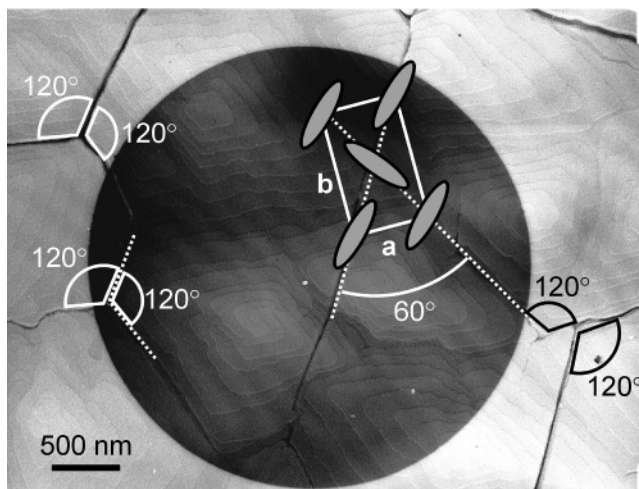


**Figure 4.** TEM image of a **CHFTTF** film deposited at a substrate temperature of 140 °C. The high substrate temperature yields a closed, smooth surface with very large crystalline grains that exhibit several fractures. The azimuths under which the cracks appear are not arbitrary, but mostly correspond to the short axis  $a$  as well as the two diagonals of the pseudo-hexagonal in-plane unit cell.

are fractures formed postdeposition, evident from the fact that the terrace edges on both sides of the gaps match exactly. The most likely origin for the occurrence of these cracks is that on cooling, mechanical stress is released which originates from the different thermal expansion coefficients of **CHFTTF** film and TEM grid. The cracks are observable by AFM on films deposited onto Si/SiO<sub>2</sub> at a  $T_{\text{sub}} = 130$  °C.

The azimuths along which the cracks appear are not arbitrary, but instead reflect the pseudo-hexagonal geometry of the in-plane unit cell. Note that the in-plane lattice would be hexagonal if the two molecules in the in-plane unit cell were not tilted against the substrate surface plane (see inset in Figure 3b). The cracks are found to be largely parallel to the short axis,  $a$ , and the two diagonals of the in-plane unit cell, directions which are separated by 60° and 120° (see Figure 4). This is also along the axis where the **CHFTTF** molecules are *most densely* packed. The correspondence between the cracks and the most densely packed lattice azimuths is not surprising, considering the fact that crystal face separation phenomena like cracks or cleavage are usually associated with a minimum surface energy configuration, i.e., favorably occur along close-packed surfaces (3D) or directions (2D). One of the cracks, visible in the upper right corner of the image, corresponds to one of the second most densely packed azimuths (equivalent to the long unit cell axis  $b$ ).

Figure 5 shows the topography MAC-AFM images of **CH4T** deposited at  $T_{\text{sub}} =$  (a) 25 °C, (b) 80 °C, and (c) 95 °C. At room temperature, the grain size ranges from 50 to 200 nm with a significant amount of morphological defects such as screw dislocations and grain boundaries. At  $T_{\text{sub}} = 80$  °C, the grains size increases to 300–500 nm. At  $T_{\text{sub}} = 95$  °C, terraced grains as large as 5 μm are observed with thickness steps of  $d = 23$  Å, consistent with single molecular stacks (**CH4T**  $d = 21.3$  Å from a MM2 calculation). XRD data for the films at all temperatures show first- and second-order diffractions at  $2\theta = 4.24^\circ$ ,  $d = 20.8$  Å, and  $2\theta = 8.52^\circ$ ,  $d = 10.4$  Å.

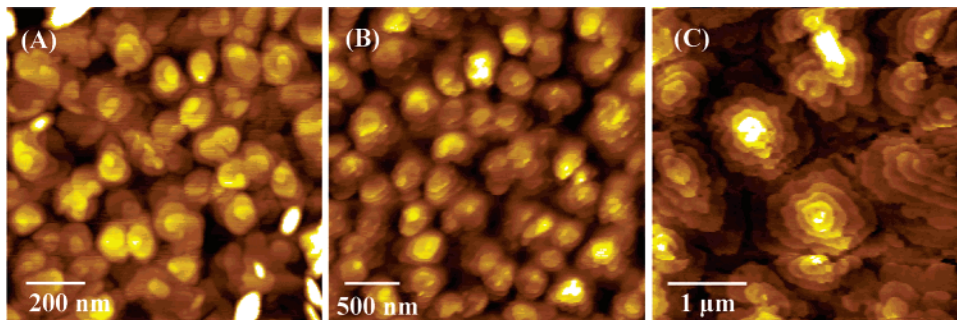


Figure 5. MAC-AFM of CH4T deposited at (a) 25 °C (topography), (b) 80 °C (topography), and (c) 95 °C (topography).

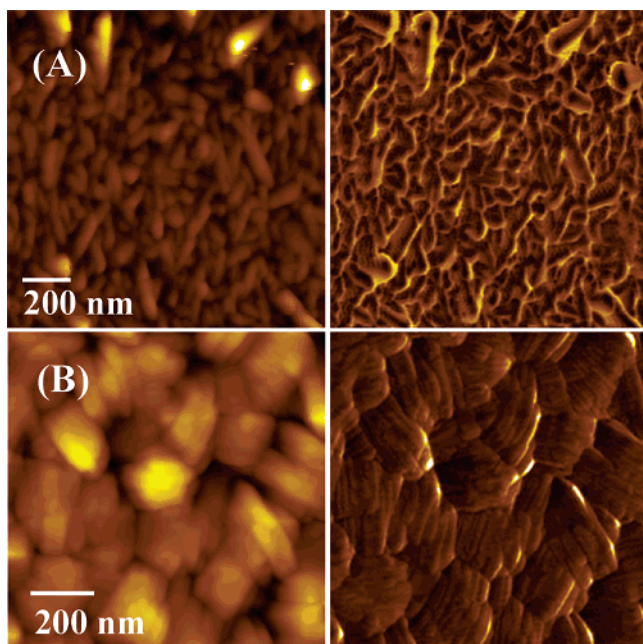


Figure 6. AFM (topography and phase) of CHPTCDI deposited at (a) 25 °C and (b) 125 °C.

Table 1. Average Field-Effect Mobility<sup>a</sup> and On/Off Ratio<sup>b</sup> for CHFTTF ( $W/L = 6$ ,  $L = 40 \mu\text{M}$ ) Deposited at Different Substrate Temperatures ( $T_{\text{sub}}$ , °C)

	25 °C	75 °C	115 °C	130 °C	150 °C
$\mu$ (cm <sup>2</sup> /V·s)	$8.7 \times 10^{-3}$	0.04	0.11	0.17	0.03
on/off ratio	$2 \times 10^5$	$5 \times 10^5$	$5 \times 10^3$	$8 \times 10^5$	$1 \times 10^3$

<sup>a</sup> Mobility is calculated using currents from the saturated regime. <sup>b</sup> On/off ratio calculated for gate voltages 0 to  $-100$  V.

Figure 6 shows the MAC-AFM topography and phase images of CHPTCDI deposited at (a) 25 °C and (b) 125 °C. The film at  $T_{\text{sub}} = 25$  °C consists of small, irregular crystallites with random orientation and a significant amount of grain boundaries. Also, no diffraction peaks were observed in the X-ray, indicating a poor crystalline structure throughout the film. When  $T_{\text{sub}}$  is increased to 125 °C, the grains begin to coalesce with a domain size of  $\sim 250$  nm. A lamellar arrangement is evident from the phase image. Two orders of diffraction ( $2\theta = 5.19^\circ$ ,  $d = 17.0$  Å,  $2\theta = 9.95^\circ$ ,  $d = 8.87$  Å) were observed in the X-ray diffraction.

**FET Behavior.** The electrical properties of films of CHFTTF, CH4T, and CHPTCDI were characterized in a TFT configuration with a 300-nm-thick SiO<sub>2</sub> dielectric on highly doped n-Si which served as the gate electrode. Two gold top contacts served as the source and drain, with the  $W/L$  ranging from 6 to 20 (where  $L = 40$ – $200 \mu\text{m}$ ) as noted

Table 2. Average Field-Effect Mobility<sup>a</sup> and On/Off Ratio<sup>b</sup> for CH4T ( $W/L = 20$ ,  $L = 200 \mu\text{M}$ ) Deposited at Different Substrate Temperatures ( $T_{\text{sub}}$ , °C)

	25 °C	60 °C	80 °C	95 °C
$\mu$ (cm <sup>2</sup> /V·s)	0.021	0.038	0.030	0.030
on/off ratio	$3 \times 10^5$	$4 \times 10^5$	$2 \times 10^6$	$1 \times 10^6$

<sup>a</sup> Mobility is calculated using currents from the saturated regime. <sup>b</sup> On/off ratio calculated for gate voltages 0 to  $-100$  V.

Table 3. Average Field-Effect Mobility<sup>a</sup> and On/Off Ratio<sup>b</sup> for CHPTCDI ( $W/L = 20$ ,  $L = 200 \mu\text{M}$ ) Deposited at Different Substrate Temperatures ( $T_{\text{sub}}$ , °C)

	25 °C	125 °C
$\mu$ (cm <sup>2</sup> /V·s)	$4.2 \times 10^{-5}$	$1.9 \times 10^{-4}$
on/off ratio	90	100

<sup>a</sup> Mobility is calculated using currents from the saturated regime. <sup>b</sup> On/off ratio calculated for gate voltages 0 to  $-100$  V.

in Tables 1–3. Representative  $I_{\text{DS}}$  vs  $V_{\text{DS}}$  at different  $V_{\text{G}}$  are shown for each oligomer in Figure 7. As expected, CHFTTF and CH4T operated in a typical  $p$ -channel accumulation regime while CHPTCDI showed  $n$ -channel behavior. There is slight leakage from the gate to the drain, which can be seen in Figure 7 close to the origin, due to both the active material and gate being unpatterned.<sup>15,16</sup> This can be improved significantly by patterning both the organic semiconductor and gate electrode. The field effect mobility,  $\mu$ , was estimated from  $I_{\text{DS}}$  in the saturation regime according to Equation 1, where  $L$  is the channel length,  $W$  is the channel width,  $C_i$  is the capacitance of the SiO<sub>2</sub> insulating layer,  $V_{\text{G}}$  is the gate voltage, and  $V_{\text{T}}$  is the threshold voltage. The mobilities at different  $T_{\text{sub}}$  are summarized in Tables 1, 2, and 3.

$$I_{\text{DS}} = \frac{WC_i}{2L} \mu (V_{\text{G}} - V_{\text{T}})^2 \quad (1)$$

From Table 1, it is evident that the observed mobility can be correlated with film morphology (grain size) and increasing crystallinity with an increasing  $T_{\text{sub}}$ . The mobility reaches  $0.17 \text{ cm}^2 \cdot \text{V}^{-1} \cdot \text{s}^{-1}$  when  $T_{\text{sub}} = 130$  °C. This is higher than the mobility observed for unsubstituted and slightly higher than hexyl-substituted FTTF.<sup>4,5</sup> The decrease in mobility at

(15) Dodabalapur, A.; Laquindanum, J.; Katz, H. E.; Bao, Z. *Appl. Phys. Lett.* **1996**, *69*, 4227.

(16) Tate, J.; Rogers, J. A.; Jones, C. D. W.; Vyas, B.; Murphy, D. W.; Li, W.; Bao, Z.; Slusher, R. E.; Dodabalapur, A.; Katz, H. E. *Langmuir* **2000**, *16*, 6054.

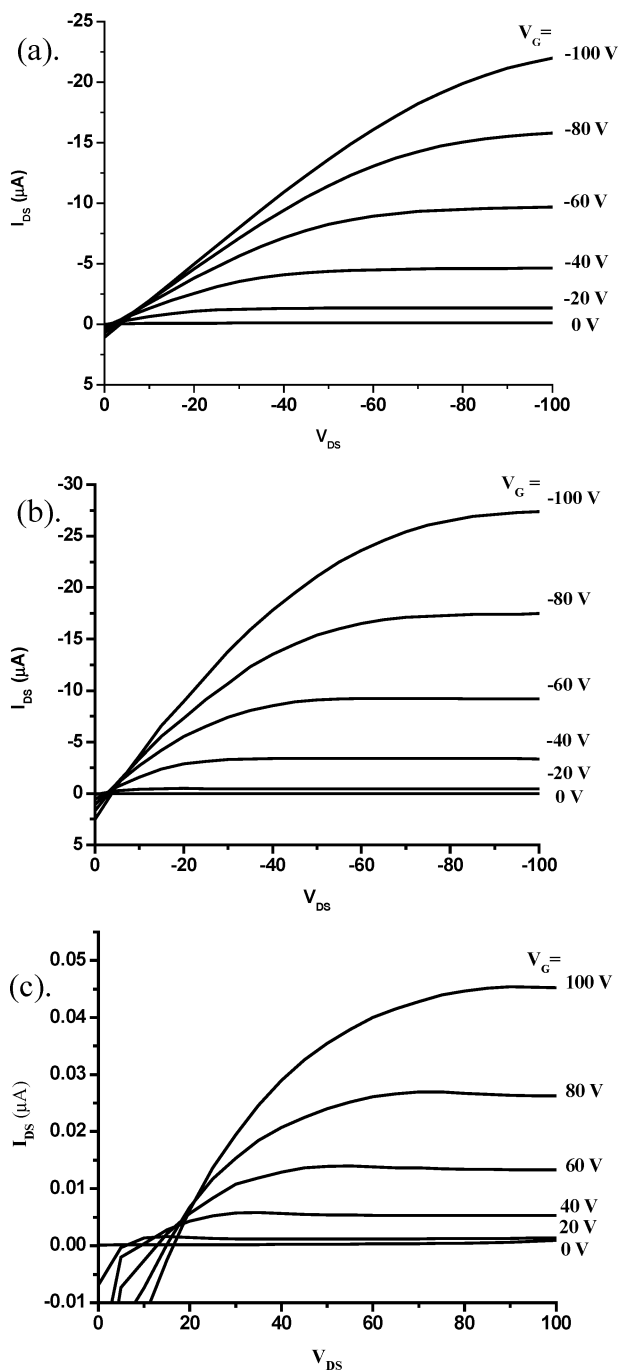


**Figure 7.** Representative  $I_{DS}$  vs  $V_{DS}$  characteristics of (a) **CHFTTF** ( $T_{sub} = 115\text{ }^\circ\text{C}$ ,  $W/L = 6$ ), (b) **CH4T** ( $T_{sub} = 60\text{ }^\circ\text{C}$ ,  $W/L = 20$ ), and (c) **CHPTCDI** ( $T_{sub} = 125\text{ }^\circ\text{C}$ ,  $W/L = 20$ ) at different gate voltages prepared at elevated substrate temperatures.

$T_{sub} = 150\text{ }^\circ\text{C}$  is probably due to the substantial amount of nonvertical growth of the molecules with respect to the substrate as described in the AFM section above. It is also possible that there is an increase in the distance between grains at the semiconductor/dielectric interface which may account for the decrease in mobility. This has been observed with copper phthalocyanines deposited at  $T_{sub}$  above  $200\text{ }^\circ\text{C}$ .<sup>17</sup>

Table 2 shows the field effect mobility of **CH4T** at various  $T_{sub}$ . This mobility is higher than that of vacuum-deposited films of dihexyl- $\alpha$ -quarterthiophene in devices with a  $W/L$

= 20. It is worth noting that Katz et al. observed a mobility of  $0.23\text{ cm}^2\text{V}^{-1}\cdot\text{s}^{-1}$  with DH4T but only with a  $W/L = 1.5$  (active area =  $4 \times 10^{-2}\text{ mm}^2$ ). When a  $W/L = 4$  (active area =  $4\text{ mm}^2$ ) was used, the mobility decreased at least 1 order of magnitude.<sup>18</sup> In a later report, a mobility of  $0.02\text{ cm}^2\text{V}^{-1}\cdot\text{s}^{-1}$  was obtained by the same group with a larger  $W/L$ .<sup>19</sup>

With **CH4T**, there is only a slight increase in  $\mu$  at elevated temperatures of deposition although the morphology of the films exhibited significant changes in grain size and structure as observed with AFM. The reason may be because of the greater chance of encountering traps or defects when such a large device is tested ( $L = 200\text{ }\mu\text{m}$ ). In each case of varying  $T_{sub}$ , the on/off ratio was exceptionally high with **CH4T**, approaching  $10^7$  at  $T_{sub} > 80\text{ }^\circ\text{C}$ .

Garnier et al. have also reported a mobility of  $0.03\text{ cm}^2\text{V}^{-1}\cdot\text{s}^{-1}$  for films spin-coated from chloroform at a substrate temperature of  $110\text{ }^\circ\text{C}$ .<sup>20</sup> This is exceptional for solution deposition and is due to the good solubility of DH4T in halogenated solvents. **CH4T** has a high solubility of  $7 \times 10^{-2}\text{ M}$  in bromobenzene at  $40\text{ }^\circ\text{C}$  and was spin-coated or drop-cast onto devices in the bottom contact geometry. Mobilities and on/off ratios as high as  $0.06\text{ cm}^2\text{V}^{-1}\cdot\text{s}^{-1}$  and  $10^5$  were obtained with **CH4T** ( $W/L = 10$ ,  $L = 25\text{ }\mu\text{m}$ ) using a drop-casting method in a closed, static atmosphere of solvent vapor similar to that reported by Katz et al.<sup>21</sup> The films fabricated by spin-coating do not show continuous morphology as observed under optical microscopy, but rather form crystals as large as  $60\text{ }\mu\text{m}$  randomly distributed over the substrate surface. More detailed studies on the solution processing of **CH4T** will be reported elsewhere.<sup>22</sup>

In the case of **CHPTCDI**, the mobilities shown in Table 3 at  $T_{sub} = 25$  and  $125\text{ }^\circ\text{C}$  are much lower than that observed with alkyl-substituted-**PTCDI** derivatives where mobilities as high as  $0.6\text{ cm}^2\text{V}^{-1}\cdot\text{s}^{-1}$  have been observed with dioctyl-**PTCDI** by Malenfant et al.<sup>23</sup> The mobility of **CHPTCDI** is similar to that of a diphenyl substituted **PTCDI** first reported by Horowitz et al.<sup>24</sup> Chesterfield et al. have recently observed a terraced structure morphology by AFM with a dipentyl-**PTCDI** grown at elevated temperature where a mobility of  $0.1\text{ cm}^2\text{V}^{-1}\cdot\text{s}^{-1}$  was obtained.<sup>25</sup> It should also be noted that Jones et al. have synthesized a perylene derivative with the core cyanated at the 1, 6, 7, and 12 positions that contains cyclohexyl substituents.<sup>26</sup> In this case, the crystal structure

(17) Bao, Z.; Dodabalapur, A.; Lovinger, A. J. *Appl. Phys. Lett.* **1996**, *69*, 306.

(18) Katz, H. E.; Lovinger, A. J.; Laquindanum, J. G. *Chem. Mater.* **1998**, *10*, 457.  
 (19) Someya, T.; Katz, H. E.; Gelperin, A.; Lovinger, A. J.; Dodabalapur, A. *Appl. Phys. Lett.* **2002**, *81*, 3079.  
 (20) Garnier, F.; Hajlaoui, R.; El Kassmi, A.; Horowitz, G.; Laigre, L.; Porzio, W.; Armanini, M.; Provasoli, F. *Chem. Mater.* **1998**, *10*, 3334.  
 (21) Katz, H. E.; Siegrist, T.; Lefenfeld, M.; Gopalan, P.; Mushrush, M.; Ocko, B.; Gang, O.; Jisrawl, N. *J. Phys. Chem. B.* **2004**, *108*, 8567.  
 (22) Locklin, J.; Mannsfeld, S. C. B.; Bao, Z. Manuscript in preparation.  
 (23) Malenfant, P. R. L.; Dimitrakopoulos, C. D.; Gelorme, J. D.; Kosbar, L. K.; Graham, T. O.; Curioni, A.; Andreoni, W. *Appl. Phys. Lett.* **2002**, *80*, 2517.  
 (24) Horowitz, G.; Kouki, F.; Spearman, P.; Fichou, D.; Nogue, C.; Pan, X.; Garnier, F. *Adv. Mater.* **1996**, *8*, 242.  
 (25) Chesterfield, R.; McKeen, J. C.; Newman, C. R.; Frisbie, C. D.; Ewbank, P. C.; Mann, K. R.; Miller, L. L. *J. Appl. Phys.* **2004**, *95*, 6396.  
 (26) Jones, B. A.; Ahrens, M. J.; Yoon, M.-H.; Facchetti, A.; Marks, T. J.; Wasielewski, M. R. *Angew. Chem., Int. Ed.* **2004**, *43*, 6363.

is influenced by the substitution of the core, and *n*-channel mobility as high as  $0.1 \text{ cm}^2\text{V}^{-1}\cdot\text{s}^{-1}$  was observed. In the case of the unsubstituted **CHPTCDI**, apparently the cyclohexyl substituents are too small to influence a packing arrangement conducive to forming large terraced grains due to the large size of the inner PTCDI core. It is an important observation that the influence of endgroup size should be taken into account when designing new organic semiconductors, especially when fused multiple aromatic ring structures are involved.

### Conclusions

In summary, we have synthesized three different oligomeric semiconductors that contain  $\alpha$ -cyclohexyl endgroups. All of the materials have appreciable solubility in halogenated solvents which may allow for better solution processability.

High mobilities were observed when oligomers were vacuum deposited at elevated substrate temperatures. Studies of the crystallinity and thin-film morphology suggest that the size of the endgroup with respect to the semiconducting core is crucial in ordering the oligomer in an end-on perpendicular alignment that is conducive to high field-effect mobility. More studies are underway regarding the influence of endgroup size and structure on the exact packing orientation and amount of intercalation when multiple layers are formed.

**Acknowledgment.** Jason Locklin thanks Lucent Technologies for a summer internship and the Director of Central Intelligence (DCI) postdoctoral research fellowship for support. Technical support from Molecular Imaging is greatly appreciated.

CM047851G